Experimental and numerical studies on a new type of bolt-ball joint for spatial grid structures

Dabin Yang[1], Mingjin Li[1], Feng Fu[2], Jinzhi Wu[3]*

1. School of Civil Engineering, Shandong Jianzhu University, Jinan 250101, China.

2. School of Mathematics, Computer Science and Engineering, City, University of London, London, UK.

3. Beijing University of Technology, Beijing 100124, China

ABSTRACT: The insufficient tightening due to workmanship and bolt loosen during the life cycle of spatial structures are common safety hazards in the installation process and the use stage of spatial structures. To tackle these problems, in this paper, a new type of bolt-ball joint with octagonal high-strength bolt is developed for conventional spatial structures. For this new type of node, the force was transmitted through the contact between the high-strength bolt and the inner wall of the octagonal sleeve, and the bolt is screwed into the bolt ball to avoid the shear forces on the pins. After installation, by checking whether the tail of the pin is flush with the outer surface of the sleeve, it will be easy to judge whether the high-strength bolt is properly tightened. To investigate the behavior of this new type of nodes, an experimental study on the tensile performance of octagonal high-strength bolts was performed. It is found that, the tensile strength of the octagonal high-strength bolts for this new type meets the requirements of the Chinese specification. Further detailed experimental studies and numerical simulations were carried out to investigate other nodes, namely steel-pipe, cone head/sealing plate nodes. The results show that the stress distribution and dimensions of the whole joints and the bearing capacity of the cone head are similar between the two nodes. The compressive test of the proposed new type of sleeve is also carried out, and the results show that the failure load is more than 3 times the required design value. Finally, the torsion bearing capacity test of this new type of node is carried out. The results show that the torsional bearing capacity of the new nodes during installation is much greater than that of the traditional ones.

***Keywords*:** bolt-ball joint, "insufficient tightening", octagonal high-strength bolts, experimental study, failure modes, numerical simulation

1. Introduction

The large-span spatial structure has been developed rapidly in the past few decades. Among them, space grid, latticed shells, etc., are the most widely used structural forms. Nodes are an essential part of single-layer grid structures. At present, more than 100 node systems have been developed in single-layer grid structures across the world [1]. Among which MERO node[2] (Fig.1), invented by Dr. Max Mengeringhausen of MERO Company in Germany in 1942, is the most famous and widely used one. Others, such as Space Deck (UK), Unistrut (US), Ohbayashi System (Japan), Unibat (France), Triodetic (Canada), and NODUS (UK), have also been promoted [3].

* Corresponding author: E-mail address: cenffu@yahoo.co.uk

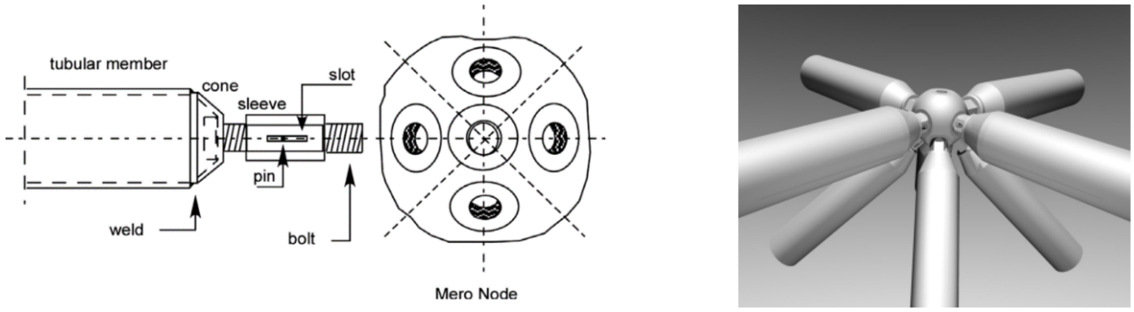

Fig.1. MERO joint.

In China, the bolt-ball joint was introduced from MERO in Germany in the 1970s. After decades of development, the joint form (Fig.2) has been formed. It has been widely used in industrial plants, stadiums, transportation hubs, terminals, and other large roof structures [4].

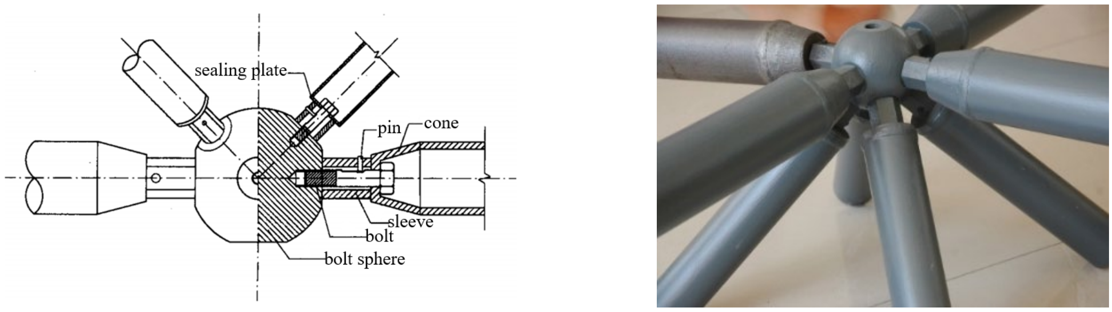

Fig.2. Traditional Chinese bolt-ball joint.

Traditional Chinese bolt-ball joints resemble MERO joints. Both bolts are driven by shear force of the pins to rotate and therefore screw into the sphere [5]. The difference is that the MERO joint has pin holes on the bolts and a sliding groove on the sleeve. During installation, the sleeve is inserted into the bolt, and the pin is inserted from the chute of the sleeve and screwed into the pin hole of the high-strength bolt. The rotating sleeve transmits the torsional force through the contact between the pin and the wall of the sleeve chute (Fig.3a), driving the bolt into the sphere until the sleeve and the surface of the bolt ball are top-tight. At this time, the pin is at the bottom of the sleeve sliding groove. By observing the state of the pin through the sliding groove, it can determine whether the pin is cut in the process of screwing. By observing the position of the pin in the sliding groove, it can determine the length of the bolt screwed into the ball. In the traditional Chinese bolt-ball joints [6], only pin holes are set on the sleeve, and sliding grooves (including deep and shallow grooves) are made on the bolts. During installation, the sleeve is inserted into the bolt, and the pin is screwed into the screw hole of the sleeve until the top end is pushed into the shallow groove of the bolt. Rotating the sleeve can transmit torque through the contact between the pin and the bolt chute wall (Fig.3b), driving the bolt to rotate together, and the bolt can be screwed into the sphere. When the sleeve and the bolt ball are tightened, the pin should reach the deep groove of the bolt. Rotate the pin again until the top end of the pin is pushed into the deep groove of the bolt.

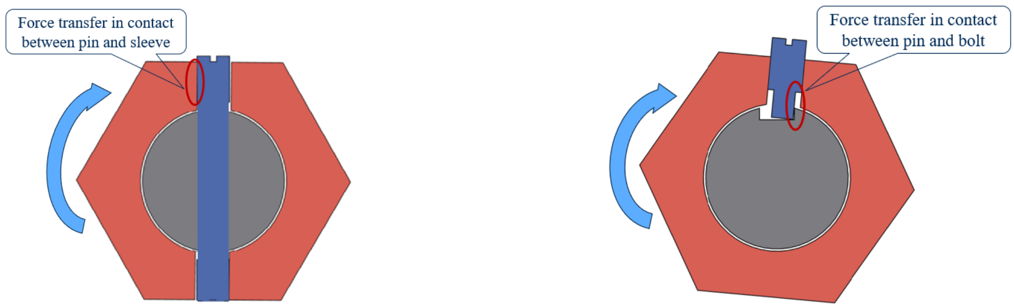

(a) MERO joint **(b) Traditional Chinese bolt-ball joint**

Fig.3. Screwing mechanism of high-strength bolt into sphere

In the traditional Chinese bolt-ball joints, when the pin is in the shallow groove of the bolt, the exposed length of the pin tail is obvious (Fig.4a). However, due to the small difference between the depth of the deep groove and the shallow groove of the traditional high-strength bolt, when the pin is rotated into the deep groove, the pin tail is still exposed, and the exposed length changes little (Fig.4b), making it impossible to judge whether the high-strength bolt is fully screwed into the bolt sphere. Even if the depth difference between the deep groove and shallow groove of the high-strength bolt is increased, the pin may have been shear off. Therefore, it is still impossible to accurately determine whether the depth of the high-strength bolt into the bolt sphere is sufficient simply based on the exposed length of the pin tail. It is impossible to judge the shear state of the pin and the screw length of the bolt screwed into the sphere through observation in the entire installation process.

(a) Pin in shallow groove **(b) Pin in deep groove**

Fig.4. Pin in shallow/deep groove status

At the construction sites, during the assembling of the space structure, construction workers often need to work on scaffolding high above-ground. However, due to the assembly error of each component, the axis of the bolt and the corresponding bolt sphere screw hole is not completely coincided, and there is a small amount of deviation. During the installation process, the installation member will be affected by its weight and the members that have been installed. The process of screwing the bolt into the bolt sphere is carried out under the condition of tension (compression) of the bolt. In the process of screwing the bolt into the bolt sphere, it is necessary to overcome the friction between the high-strength bolt thread and the inner thread of the bolt sphere. Therefore, the worker needs to use a large torque to screw the bolt into the bolt sphere. When the pin is subjected to excessive shear force, it will be sheared off, which will cause the high-strength bolt to be insufficiently screwed into the bolt sphere and “insufficient tightening” will occur, as shown in Fig.5. During the service period , “insufficient tightened high-strength bolts cannot effectively bear the tension due to the insufficient depth of the bolt screwed into sphere, and it is easy to be pulled out. This is one of the key safety hazards and accidents inducements commonly existing in the grid structure of the bolt-ball joint. Several engineering accidents are directly related to the "insufficient tightening" phenomenon of high-strength bolts. In a space grid project in Tianjin City, due to the insufficient screwing depth of a bolt, one of the web members was loosened, which induced the collapse of the structure [7]. In the lecture hall of a medical college in Shanxi province, due to the fracture of a pin, the sleeve can rotate freely, and there is a large gap between the sleeve and the bolt sphere, which causes the collapse of the grid [8].In Inner Mongolia Xin Feng Power Plant 1# steam turbine room, a space grid did not meet the requirement of Chinese code due to inadequate tightening of some high-strength bolts [9] and there were large gaps (2~25mm) between some bolts and sleeves [10], resulting in collapse. To tackle the "insufficient tightening" issues, this paper presents a new anti-insufficient tightening bolt-ball joint for spatial grids (Fig.6). By designing the form and size of bolts, sleeves, cones/sealing plates and pins, the screwing mechanism of the bolts is changed. After installation, the depth of the high-strength bolt screwed into the sphere can be determined only by directly inspection the exposed length of the pin tail.

Fig.5. The insufficient tightening of the bolt-sphere joints of grid structures.

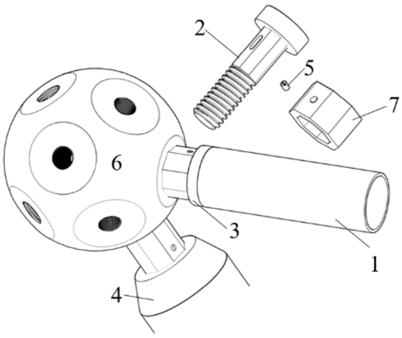

Fig.6. Visual anti-insufficient tightening bolt-ball joint for spatial grid structure[11].

2. New bolt-ball joint design

2.1 The composition and innovation of new bolt-ball joint

The new bolt-ball joint (Fig. 6) consists of bolt sphere (denoted as 6), high-strength bolt (denoted as 2), sleeve (denoted as 7), cone head (denoted as 4)/ sealing plate (denoted as 3), pin (denoted as 5) and other accessories. The force transfer path is consistent with the traditional bolt-ball joint. When members in spatial grids are subjected to tension, the load path is as follows: tensile force → steel pipe → cone head/sealing plate → bolt → bolt sphere. When members are subjected to compression, the load path is as follows: pressure force → steel pipe → cone head/sealing plate → sleeve → bolt sphere [12].

Compared with the traditional bolt-ball joint, the main innovations of the proposed new bolt-ball joint are as follows :(1) The mechanism of the high-strength bolts screwing into the bolt sphere is different. In the new bolt-ball joint (Fig.7), the cross-section of the shank of the bolt is adapted into polygonal shape rather than the traditional circular shape, the movement of the bolts relies on rotating the sleeve so that the polygonal shank of the high-strength bolt is in contact with the inner wall of the sleeve (also made in polygonal shape) to transfer torque and screw the bolt into the sphere. In this process, the pin and the bolt chute will not contact each other. Therefore, the pin is not stressed. (2) After the assembly of the new bolt-ball joint, the screwing depth of the high-strength bolt can be judged by inspection of the exposed length of the pin tail. When the pin is located in the shallow groove of the bolt, the exposed length of the tail is apparent (Fig.8a). When the pin is screwed into the deep hole of the bolt, its tail is flush with the sleeve surface and not exposed (Fig.8b), indicating that the high-strength bolt is completely screwed into the ball.

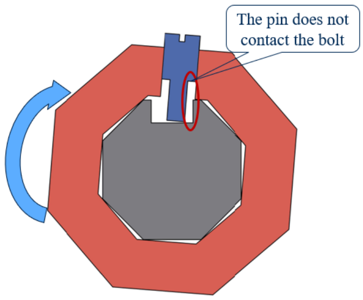

Fig.7. Screwing mechanism of high-strength bolt into sphere

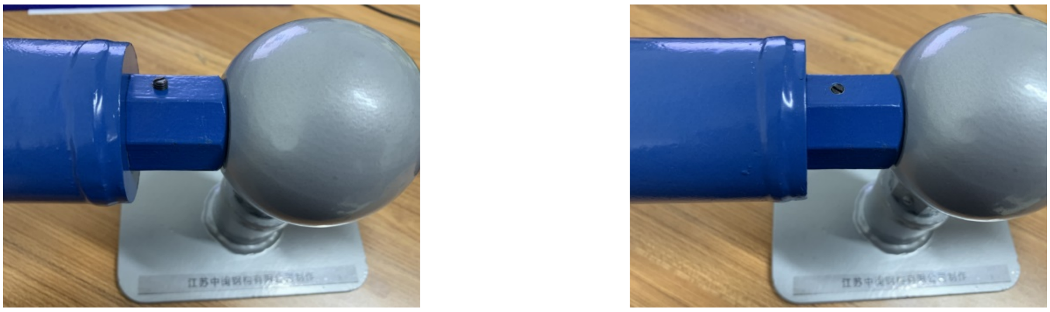

(a) Pin in shallow groove **(b) Pin in deep hole**

Fig.8. Pin in shallow/deep groove (hole) status of the new joint

2.2 Design of high-strength bolts

2.2.1 Determination of polygon edge numbers of high-strength bolts

The polygon segment of the high-strength bolt is determined based on the same inscribed circle with a nominal diameter of the thread segment. The number of sides of the regular polygon is preliminarily designed as 6, 8, and 10, as shown in Fig.9a. Because the shape of decagon is the most complicated, the workmanship of the size of the bolt and the sleeve are the highest, and the size errors can easily lead to slippage between decagonal bolts and sleeves during rotation. Therefore, the decagon is not used in the proposed new joints.

For the same type of high-strength bolt, the hexagonal and octagonal segment and their inscribed circles and circumscribed circles are shown in Figure 8b, where both the inscribed circle diameters are the same as the nominal diameter of the bolt thread segment. The aperture of the circumcircle of the hexagon is enlarged by about 15% compared with the nominal diameter of the bolt, while that of the octagon is only 8%. After the bolt is put into the cone head, the contact surface of different types of bolts nuts and the cone plate is shown in Fig.9c-e. The contact area reduction table is shown in Table 1. It can be concluded that the hexagon bolt contact surface reduction rate is about 2 times that of the octagonal bolt contact surface reduction rate. The contact area between the bolt and the cone head/sealing plate is too small, thus reducing the tensile bearing capacity of the conical head/sealing plate. Therefore, the octagon is chosen as the polygon section of the high-strength bolt.

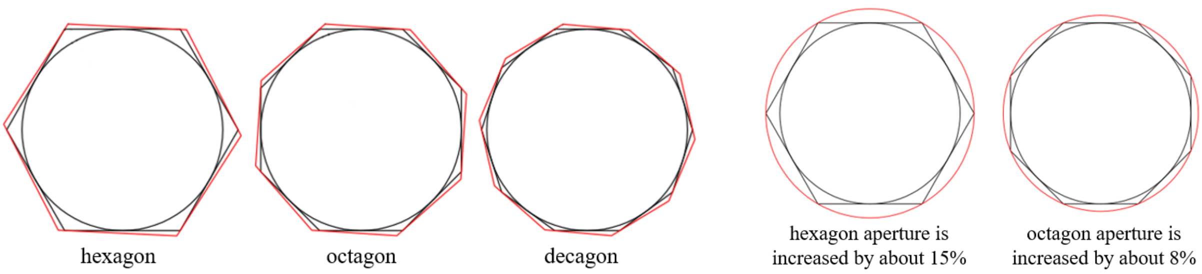

(a) Comparison of different polygon sides **(b) Hexagonal and octagonal segments**

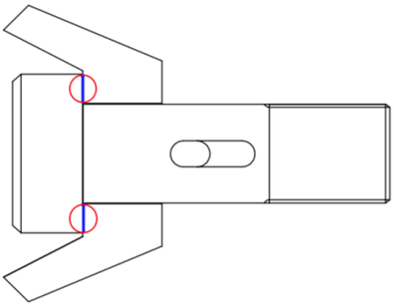

(c) Traditional bolts

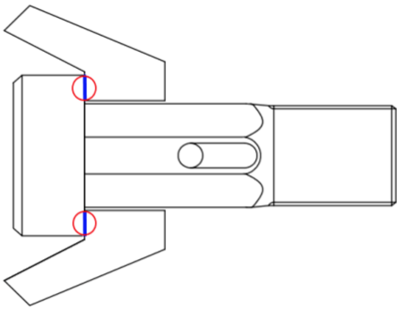

(d) Octagonal bolts

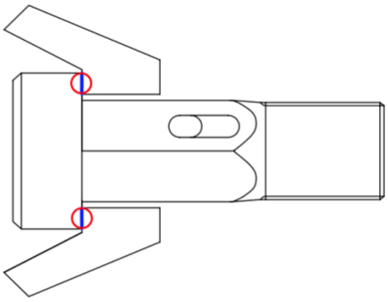

(e) Hexagonal bolts

Fig.9. Contact surface of different bolt nuts and cone heads

Table 1

Contact area reduction table for different types of bolts and cone head.

Cone head type	Contact area of traditional bolts/cone head (mm²)	Contact area of hexagon bolts/cone head (mm²)	Area reduction rate (%)	Contact area of octagonal bolts/cone head (mm²)	Area reduction rate (%)
ZT75.5-3.75-20	360.315	254.34	-29.41	309.09	-14.22
ZT114-4-36	1299.96	956.72	-26.40	1118.63	-13.95
ZT159-6-45	2185.44	1641.44	-24.89	1923.05	-12.01
ZT168-8-56	3808.035	2990.65	-21.46	3389.43	-10.99

2.2.2 Design of the bolts

The form of the octagonal high-strength bolt is shown in Fig.10.

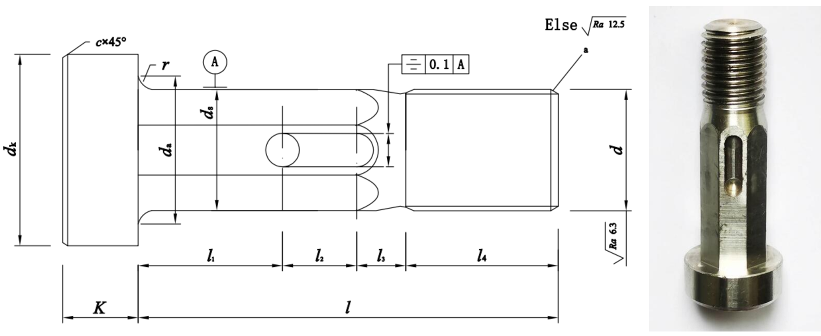

Fig.10. Octagonal high-strength bolt

Where *K* is the nut thickness; d_k is the diameter of the nut; d_a is the length between the bolt member and the nut chamfer; d_s is the length of the opposite side of the octagon screw; *d* is the diameter of the bolt; l_1 is the length from the bottom of the nut to the center of the deep hole; l_2 is the length of the chute; l_3 is the transition length between octagonal screw and thread segment; l_4 is the length of the thread segment.

2.3 Cone head/sealing plate design

The form of cone head/sealing plate of the new joint is the same as that of the traditional joint. The hole diameter of the traditional cone head/sealing plate is 1mm larger than the nominal diameter of the corresponding bolt (Fig.11a). When the octagonal bolt of the same nominal thread diameter is used, the traditional hole can no longer accommodate the octagonal high-strength bolts. Therefore, it is necessary to increase the size of opening circular hole diameter of the cone head/sealing plate to adapt to the octagonal high-strength bolt (Fig.11b).

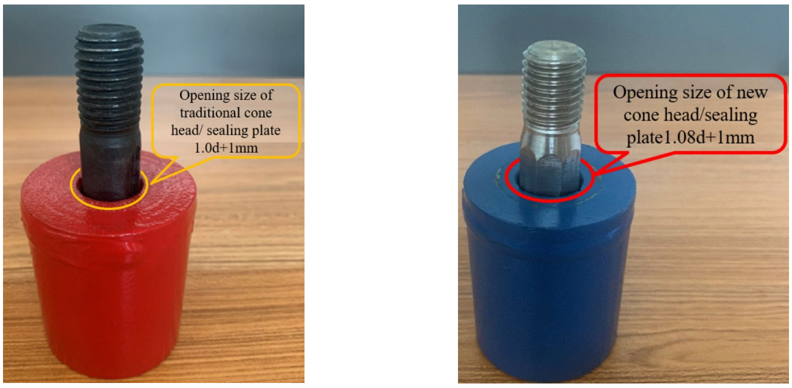

(a) Traditional joints **(b) New joints**

Fig.11. Opening circular holes of cone head/sealing plate

2.4 Sleeve

The design principles of the sleeve are as follows: (1) The distance between the opposite sides of the octagon in the sleeve section is 1mm or 0.5mm (MY20 and below) larger than the distance between the opposite sides of the octagon section of the high-strength bolt. (2) Sleeve wall thickness *h* (Fig.12) is mainly determined from the following three aspects: 1) Bearing capacity is equivalent to the corresponding traditional sleeve bearing capacity. 2) The high-strength bolt is tightened, and the pin is flush with the sleeve. 3) The types of pins should not be too many. The sectional view of the sleeve is shown in Fig.11.

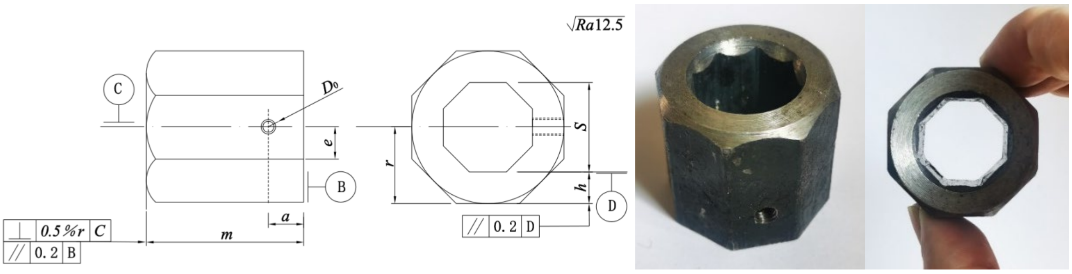

Fig.12. Sleeve.

Where *m* is the total length of the sleeve; D_0 is the pin aperture; *e* is the distance from the center of the pin hole to the edge of the outer octagon; *S* is the distance between the opposite sides of the octagon in the sleeve; *a* is the distance from the center of the pin hole to the end of the sleeve.

2.5 Pin

The total length *L* of the pin is determined by Fig.13a and formula (1) below. The form of the pin is shown in Fig.13b.

$$L = h + t_1 + t_2 \tag{1}$$

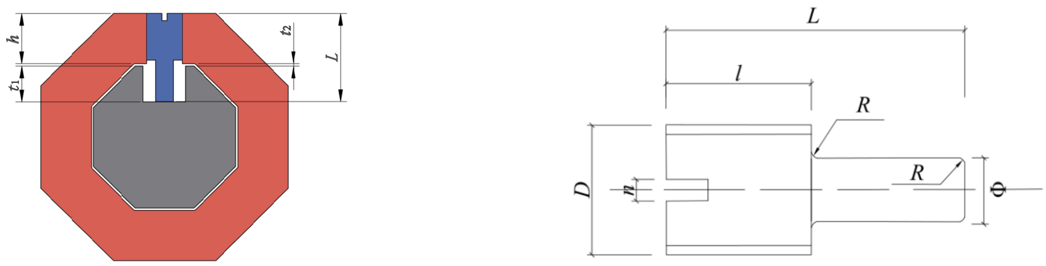

(a) End screw position of pin **(b) Pin detail**

Fig.13. Pin.

Where D is the diameter of the pin end; l is the length of the pin thread section; Φ is the diameter of the pin head.

3. Experimental study on tensile strength of octagonal high-strength bolts

"High strength bolts for joints of space grid structures" in Chinese (GB/T 16949-2016) require that high-strength bolts should be screwed into the internal threads of a special anchor in a tensile test so that the length of the screw is not less than 6P (Where P is the distance between a point on a screw thread and the corresponding point on the adjacent screw thread, and the screw length not less than 6P is the actual use of the simulated bolt). The length of unscrewed thread is not less than 2P. A wedge is placed under the bolt head. When the test tension reaches the specified range, the bolt shall break at the threaded part of the junction between the thread and the screw [13].

3.1 Materials, dimensions, and loading equipment for octagonal high-strength bolts

Four commonly used types of octagonal high-strength bolts were designed: MY20, MY36, MY45, and MY56. A total of 12 samples were prepared for 3 samples of each type. The materials and dimensions of octagonal high-strength bolts are shown in Table 2.

Using 100t hydraulic tensile testing machine (Fig.14b) for MY20, MY36 high-strength bolts tensile load test. Using 300t horizontal tensile testing machine (Fig.14a) for MY45, MY56 high-strength bolts tensile load test. Screw the specimen into a special fixture (Fig.14c) and load it on the test machine (Fig.14d).

Table 2

Materials and dimensions of octagonal high-strength bolts.

Bolt	Strength grade	Material	l(mm)	d_k(mm)	d(mm)	K(mm)
MY20	10.9S	40Cr	73	31	20	12.5
MY36	10.9S	40Cr	125	57	36	22.5
MY45	9.8S	40Cr	145	72	45	28
MY56	9.8S	40Cr	172	92	56	35

(a) 300t horizontal tensile testing machine

(b) 100t hydraulic tensile testing machine **(c) Anchor** **(d) Sample loading**

Fig.14. Test equipment.

3.2 Experimental result

When the octagonal high-strength bolt reaches the ultimate tensile strength, the bolt fracture failure occurs as shown in Fig.15, and the load-displacement curve is shown in Fig.16. The fracture of MY20 extends in the direction of 60° at the junction of thread and screw (Fig.15a), and the other three groups are all fractured at the junction of thread and screw. The fracture surface is smooth (Fig.15b-d), which is the same as the fracture location and shape of high-strength bolt tests in other documents [14]. According to the test results in Table 3: Except for the tensile load of one sample in MY45, which exceeds 2.36% of the maximum tensile load specified in the standard, the failure load, failure position, failure form, and elongation of the other octagonal high-strength bolts all meet the requirements of the current standard "High strength bolts for joints of space grid structures" in Chinese (GB/T 16949-2016) [13]. Therefore, the tensile capacity of octagonal high-strength bolts meets the requirements.

(a) MY20 **(b) MY36** **(c) MY45** **(d) MY56**

Fig.15. Failure mode.

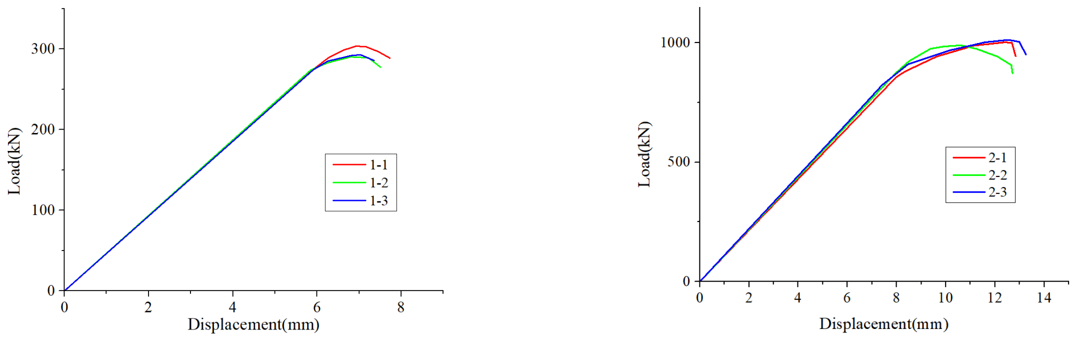

(a) MY20 **(b) MY36**

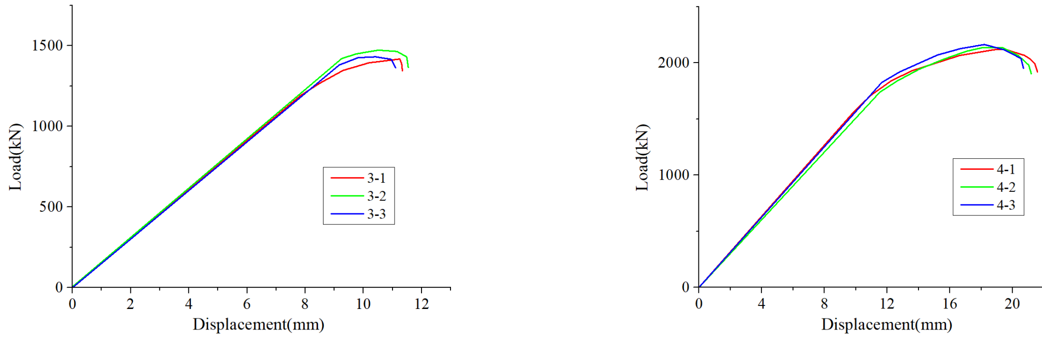

(c) MY45 **(d) MY56**

Fig.16. The load-displacement curve of the bolt.

Table 3

Experimental results.

Bolt	Number	Tensile load (kN)	The code requires the tensile load range (kN)	Failure location and failure form	Elongation (%)	The specification requires elongation (%)	Meets specification requirements (T/F)
MY20	1-1	302	255～304	The joint between the thread and the screw is extended and fractured in the direction of 60°	11.84	≥10	T
	1-2	290			12.87		T
	1-3	291			10.16		T
MY36	2-1	1003	850～1013	Smooth fracture at the junction of thread and screw	10.48		T
	2-2	991			10.46		T
	2-3	1011			10.86		T
MY45	3-1	1408	1179～1441		10.31		T
	3-2	1475			10.38		Tensile load beyond the normal tensile range
	3-3	1422			10.15		T
MY56	4-1	2128	1930～2358		12.62		T
	4-2	2152			13.96		T
	4-3	2163			12.50		T

4. Bearing capacity of cone head

Under different stress conditions, the bolt-ball joint has different force transmission paths and acting parts. When the member is under pressure, the pressure between the sleeve and the cone head is transmitted along with the cone shell, which is equivalent to the cone shell bearing the in-plane pressure. When the member is under tension, the tensile force between the bolt and the cone head is transferred by the nut and the cone head top plate, and the cone head top plate is subjected to the out-of-plane force. For shell-plate structure, the in-plane strength of the shell is higher than the out-of-plane strength of the plate. Therefore, the bearing capacity of the cone head is higher under compression than under tension. The cone head plate in the new bolt ball joint has to meet the requirements of octagonal high-strength bolts, which increases the hole diameter (Fig.11b). As the size of the cone head has changed, it is necessary to study the bearing capacity of the cone head.

Zhang et al. [15] studied the theoretical analysis and simplified calculation of the strength of the cone head (Fig.17). The obtained the approximate formula (2) for calculating the tensile design bearing capacity of the cone head：

$$[N]=0.4487\cdot(D)^{1.73534}\cdot(k)^{-0.399}\cdot(h/H)^{0.6926}\cdot(s)^{0.26034}\cdot f \quad (2)$$

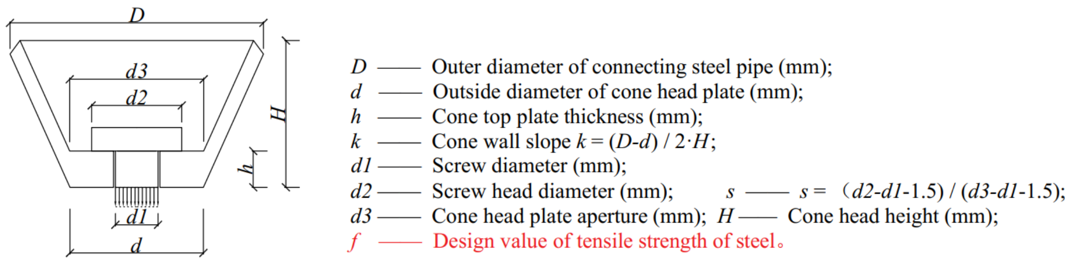

Fig.17. Schematic of cone head calculation.

Where: 88.5mm≤D≤275mm, 0.15≤$d1/D$≤0.4,0.5≤d/D≤0.7, 0.2≤k, h/H≤0.5,0.25≤S≤1.0, N unit is Newton (N).

Based on this formula, it can be seen that the relationship between the tensile design bearing capacity of the cone head N and the parameter s is positively correlated. Therefore, take the screw diameter $d1$ as the independent variable and s as the dependent variable, and take the derivative of s, as shown in formula (3).

$$\frac{\mathrm{ds}}{\mathrm{d}(d1)}=\left(\frac{d2\text{-}d1\text{-}1.5}{d3\text{-}d1\text{-}1.5}\right)'=\frac{(-1)\cdot(d3\text{-}d1\text{-}1.5)\text{-}(-1)\cdot(d2\text{-}d1\text{-}1.5)}{(d3\text{-}d1\text{-}1.5)^2}=\frac{d2\text{-}d3}{(d3\text{-}d1\text{-}1.5)^2}<0 \quad (3)$$

The derivative result is negative, indicating that the screw diameter $d1$ is negatively correlated with s. Which is the screw diameter $d1$ is negatively correlated with the tensile design bearing capacity of the cone head. Therefore, the increase of screw diameter $d1$ is unfavorable to the tensile design bearing capacity of the cone head. The outer diameter of the connecting steel pipe D, the thickness of the top plate h, and the diameter of the screw head $d2$ are positively correlated with the tensile design bearing capacity of the cone head. In order not to increase the cost, the manufacturing mold of the cone head is not changed, only the opening size of the cone head is changed. In the design of high-strength bolts with new bolt-ball joints, by increasing the diameter $d2$ of the screw head, the problem of the reduced tensile design bearing capacity of the cone head due to the increase of the screw diameter $d1$ is solved.

Expand the screw head diameter of MY16~MY30 bolts by 1mm, and expand the screw head diameter of MY36~MY85 bolts by 2mm. According to the order of bolt models from small to large, 9 kinds of matching cone heads made of Q235 are selected, according to formula (2), carrying out the calculation of the tensile design bearing capacity of the cone head. The calculation results are shown in Table 4. In addition to the taper head model ZT89-4-20 tensile design bearing capacity decreased, the other models are slightly improved. It shows that increasing the diameter $d2$ of the screw head by a certain range can slightly increase the bearing capacity of the cone head, offsetting the reduction of the tensile design bearing capacity due to the enlargement of the cone head opening hole.

Table 4

Comparison of tensile design bearing capacity of cone head before and after reaming.

Steel material	Cone head type	Change in diameter of cone head after reaming (mm)	Hole expansion rate (%)	Length of original screw head	Length of expansion head diameter	Original tensile strength (kN)	Tensile strength after reaming	increasing rate (%)
Q235B	ZT89-4-20	1.5	7.14	30	31	158.47	156.46	-1.27

Q235B	ZT108-4-27	2	7.14	41	42	210.21	210.58	0.17
Q235B	ZT140-4.5-30	2.5	8.06	46	49	306.92	307.67	0.24
Q235B	ZT159-6-36	3	8.1	55	57	418.98	428.32	2.23
Q235B	ZT168-8-42	3.5	8.14	65	67	504.14	513.36	1.83
Q235B	ZT180-8-42	3.5	8.14	65	67	581.52	592.15	1.83
Q235B	ZT194-10-56	4.5	7.9	90	92	742.86	752.84	1.34
Q235B	ZT219-8-48	4	8.16	75	77	681.24	691.81	1.55
Q235B	ZT245-10-64	5.5	8.46	100	102	963.35	975.364	1.25

Note: The cone head model ZT89-4-20 means that the diameter of the cone head connecting steel pipe is 89mm, the thickness is 4mm, and the matching bolt model is M20.

5. Steel pipe - Cone head /sealing plate and bolt integral test

The slope k of the cone wall of the cone head in the theoretical calculation of the tensile design bearing capacity of the cone head is a fixed value, assuming that the cone wall of the cone head is of equal thickness. Fig.18 shows the cone head used in real construction projects. The slope k of the inner cone head wall and the outer cone head wall of the cone head are different. The cone head wall is not of equal thickness, and the thickness of the cone head wall increases from the junction with the pipe to the top plate of the cone head. Therefore, only using the theoretical formula (2) to analyze the tensile design bearing capacity of the cone is deviated. It is necessary to carry out the overall test of the steel pipe-cone head/sealing plate and bolts to further analyze the influence of the increase in the size of the cone head opening and the increase in the diameter of the screw head on the tensile bearing capacity of the cone head and the overall test piece.

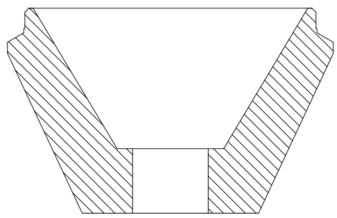

Fig.18. Cone head used in real construction projects

In the test, the bolt type selected is commonly used in actual projects and the corresponding member. The elastic stiffness, failure mode, and failure load of the new bolt-ball joint and the traditional bolt-ball joint were compared by selecting typical bolts from each type of bolt by setting a control test. The bolt type, steel pipe type, size, and material selected in the test are shown in Table 5. Fig.19 is the schematic diagram of test loading, and Fig.20 is the loading device.

Table 5

Type of bolt, type of steel pipe, size, and material.

Bolt	**Strength grade**	**Bar type**	**Materials**	***d* (mm)**	***B* (mm)**	**d_1 (mm)**	**d_2 (mm)**	**d_3 (mm)**	***L* (mm)**
M20	10.9S	Φ60×3.5	Q355	20	18	21	60	53	250
		Φ75.5×3.75	Q355				75.5	68	
MY20	10.9S	Φ60×3.5	Q355			21.5	60	53	
		Φ75.5×3.75	Q355				75.5	68	
M36	10.9S	Φ114×4	Q235	36	30	37	114	106	

		Φ114×4	Q355				114	106
		Φ140×4.5	Q235				140	131
MY36	10.9S	Φ114×4	Q235		30	40	114	106
		Φ114×4	Q355				114	106
		Φ140×4.5	Q235				140	131
		Φ159×6	Q235				159	147
M45	9.8S	Φ159×6	Q235	45	36	46	159	147
MY45	9.8S	Φ159×6	Q235			49.5	159	147
		Φ159×8	Q235				159	147
		Φ159×10	Q235				159	139
M56	9.8S	Φ180×12	Q235	56	45	57	180	156
MY56	9.8S	Φ159×8	Q355			61.5	159	151
		Φ180×12	Q235				180	156

Note: The type of member is ΦA×B, where ΦA represents the diameter of the member and B represents the thickness of the steel pipe.

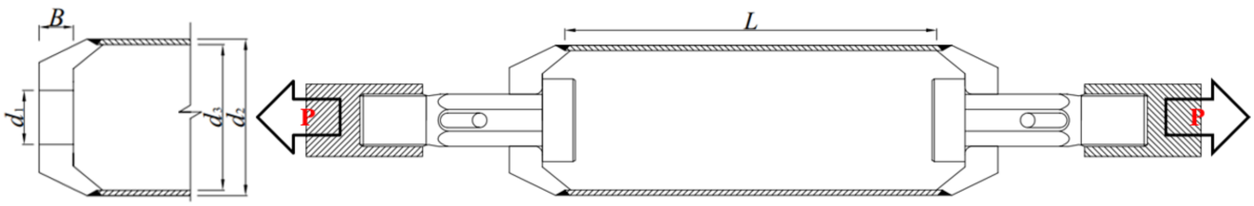

Fig.19. Test loading instructions.

(a) 100t hydraulic tensile testing machine **(b) 300t horizontal tensile testing machine**

Fig.20. Loading device.

The depth of high-strength bolt screw-in fixture meets the requirements of "Technical specification for space frame structure" in Chinese (JGJ7-2010) [8] of 1.1 times bolt diameter *d*. There are 26 new bolt-ball joint specimens and 13 traditional bolt-ball joint specimens, a total of 39 specimens. Fig.21 shows the three failure modes of specimens: (1) Steel pipe failure: When the steel pipe reaches the ultimate tensile strength, the steel pipe is broken from the middle part, and there is an obvious necking phenomenon. Before the fracture, there is a "thumping" sound, and when it breaks, it makes a "pop" sound. (2) Bolt failure: The high-strength bolt reaches the ultimate tensile strength, and the failure position is at the junction of the screw and the threaded section. There is no apparent necking phenomenon. It is consistent with the previous literature [16-17], and it makes a huge noise when it fails. (3) Weld failure: Two of the 39 specimens fractured from the weld, but the failure load was also within the calculated failure load range of the member, indicating that the quality of the weld between the steel pipe and the cone satisfied the "Standard for construction quality of steel structure" in Chinese (GB 50205-2020) [18] and other strength connection requirements. There was no failure of cone head/sealing plate in all test schemes, and the failure position and load of each specimen were shown in Table 6. Fig.22 shows the failure of the specimen with new joints, and Fig.23 shows the load-displacement curve of the specimen.

(a) Steel pipe damage (MY36 Φ114×4-1) **(b) Bolt damage (MY56 Φ180×12-1)** **(c) Weld damage (MY45 Φ159×6-2)**

Fig.21. Failure mode.

Table 6

Failure mode.

Bolt	Bar type	Number	Materials	Damage location	Failure control components/ specification require tension load range (kN)	Tensile load (kN)
MY20	Φ60×3.5	1	Q355	Bolt	Bolt /255~304	283
		2	Q355	Bolt		279
	Φ75.5×3.75	1	Q355	Bolt	Bolt /255~304	282
		2	Q355	Bolt		292
		3	Q355	Bolt		289
M20	Φ60×3.5	1	Q355	Bolt	Bolt /255~304	268
		2	Q355	Bolt		282
	Φ75.5×3.75	1	Q355	Bolt	Bolt /255~304	267
		2	Q355	Bolt		274
		3	Q355	Bolt		288
MY36	Φ114×4	1	Q235	Steel pipe	Steel pipe /518~635	593
		2	Q235	Steel pipe		570
	Φ140×4.5	1	Q235	Steel pipe	Steel pipe /718~881	872
		2	Q235	Steel pipe		877
	Φ159×6	1	Q235	Bolt	Bolt /850~1013	974
		2	Q235	Bolt		1010
M36	Φ114×4	1	Q235	Steel pipe	Steel pipe 518~635	567
		2	Q235	Steel pipe		569
	Φ114×4	1	Q355	Steel pipe	Steel pipe /677~857	759
		2	Q355	Weld		704
MY45	Φ159×6	1	Q235	Steel pipe	Steel pipe /1081~1326	1315
		2	Q235	Weld		1323
		3	Q235	Steel pipe		1251
	Φ159×8	1	Q235	Bolt	Bolt /1179~1441	1439
		2	Q235	Bolt		1435

		3	Q235	Bolt		1433
	Φ159×10	1	Q235	Bolt	Bolt /1179~1441	1426
		2	Q235	Bolt		1432
		3	Q235	Bolt		1421
M45	Φ159×6	1	Q235	Steel pipe	Steel pipe /1081~1326	1243
		2	Q235	Steel pipe		1211
MY56	Φ159×8	1	Q235	Steel pipe	Steel pipe /1423~1745	1739
		2	Q235	Steel pipe		1707
	Φ159×8	1	Q355	Steel pipe	Steel pipe /1857~2352	1857
		2	Q355	Steel pipe		1862
	Φ180×12	1	Q235	Bolt	Bolt /1930~2358	2193
		2	Q235	Bolt		2191
M56	Φ180×12	1	Q235	Bolt	Bolt /1930~2358	2138
		2	Q235	Bolt		2241

(a) MY20

(b) MY36

(c) MY45

(d) MY56

Fig.22. Failure diagram of each specimen.

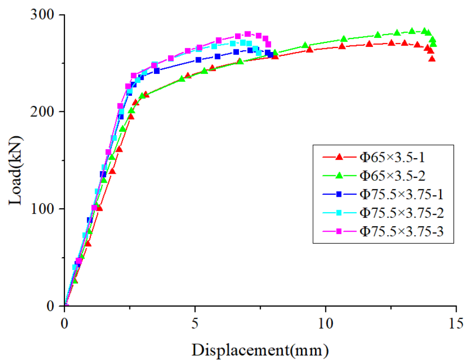

(a)MY20

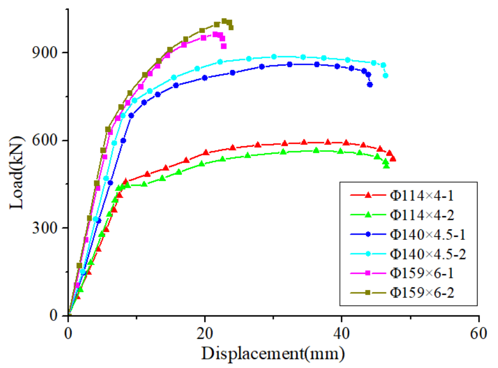

(c)MY36

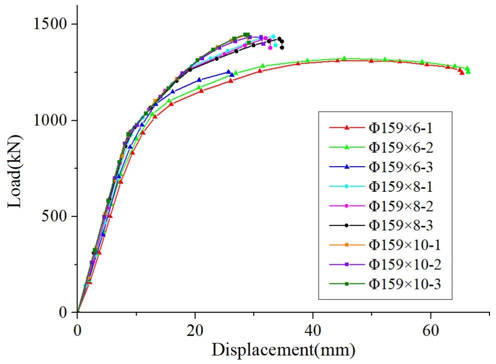

(d)MY45

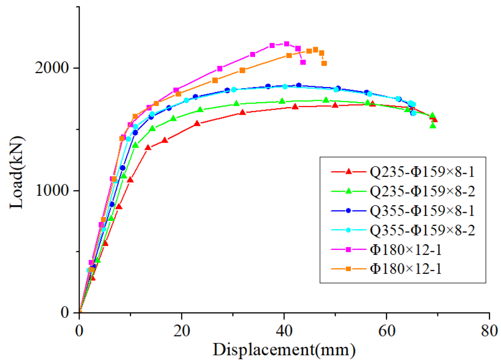

(e)MY56

Fig.23. The load-displacement curve of each specimen.

Fig.24 shows the failure modes and average load-displacement curve of traditional and new joint specimens with the same bolt type and typical bar type. It can be seen from the figure that the load-displacement curves of the traditional joint specimens with the same kind of bolt and the new joint specimens are the same, the elastic stiffness is similar, and the load to enter the plasticity is identical. But the ultimate tensile strength of the whole specimen of the new bolt is slightly higher than that of the entire specimen of the traditional high-strength bolt.

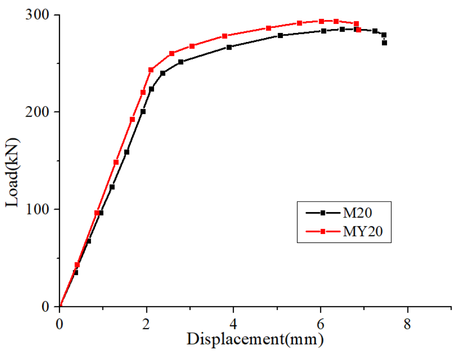

(a) Φ75.5×3.75/M20—MY20

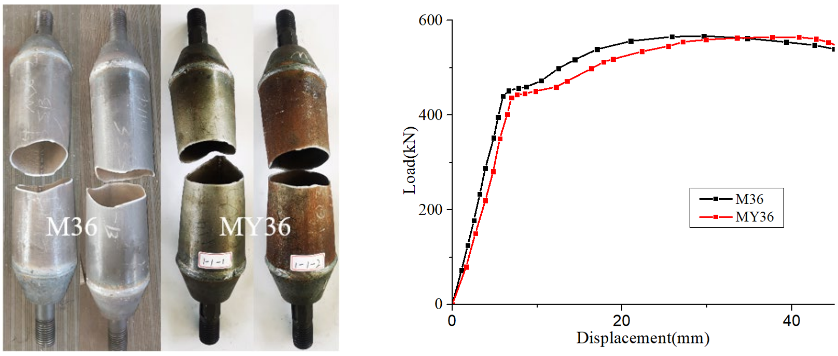

(b) Φ114×4/M36—MY36

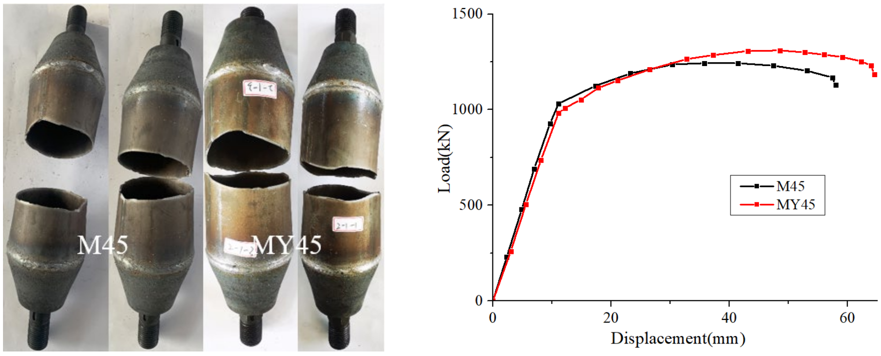

(c) Φ159×6/M45—MY45

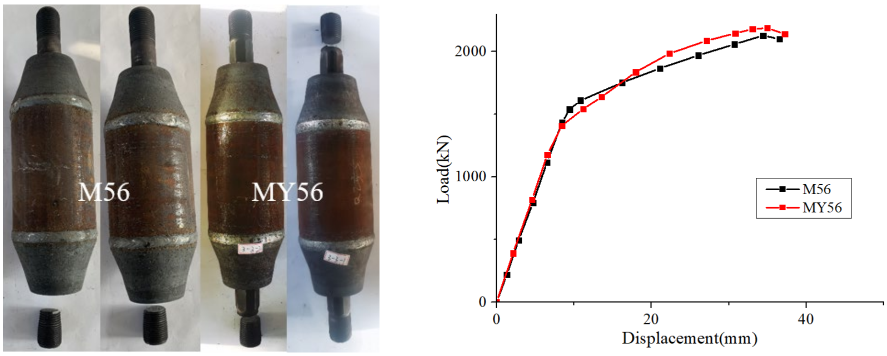

(d) Φ180×12/M56—MY56

Fig.24. Failure diagram and load-displacement curve of typical specimens.

6. Compressive test of sleeve

The cross-section of the traditional sleeve is circular, and the radial pressure is more uniform. The pressure failure occurs in the center of the pin hole. The inner section of the new sleeve is an octagon, and the pin hole opened by the sleeve is on one face of the octagon. Under pressure, the face with the pin hole is weakened. Therefore, it is necessary to study the compression bearing capacity of the sleeve further.

6.1 Test set up

Three sleeves corresponding to MY20 of Q355 material were selected to carry out the radial compressive bearing capacity test of the sleeves. The compressive bearing capacity of the sleeve is the smaller value of the pressure on the end face of the sleeve end and the bolt-ball and the net section pressure at the location of the pin hole of the sleeve. Firstly, the design pressure value of sleeve end face N_{ce} was calculated according to formula (4). Then the design pressure value of sleeve net section N_n was calculated according to formula (5).

$$N_{ce}=\left[\pi\left(\frac{S}{2}+h\right)^2-8\left(\frac{S}{2}\right)^2\cdot\tan 22.5°\right]\cdot f_{ce} \tag{4}$$

$$N_n=\left[8\left(\frac{S}{2}+h\right)^2\cdot\tan 22.5°-8\left(\frac{S}{2}\right)^2\cdot\tan 22.5°-h\cdot D_0\right]\cdot f \tag{5}$$

Where D_0 is the pin aperture; S is the distance between the opposite sides of the octagon in the sleeve; h is sleeve thickness; f_{ce} is the design value of end-face pressure strength; f is the design value of compressive strength.

Through calculation, the design value of net compressive bearing capacity of sleeve corresponding to MY20 is 214kN, and the design value of end-face bearing capacity is 234kN. Therefore, the control value of compressive bearing capacity is 214kN. The loading device was carried out on the microcomputer-controlled electro-hydraulic servo universal testing machine, as shown in Fig.25a. Fig.25b is the schematic diagram of the sleeve compressive bearing capacity test, and Fig.25c is the diagram of the sleeve compressive test. Above all, load the design value of the sleeve compression bearing capacity, observe the deformation of the sleeve. Then load the design value 2 times, following the deformation of the sleeve. Finally, load the sleeve to failure, test its ultimate compressive bearing capacity.

(a) Microcomputer controlled electro-hydraulic servo universal testing machine

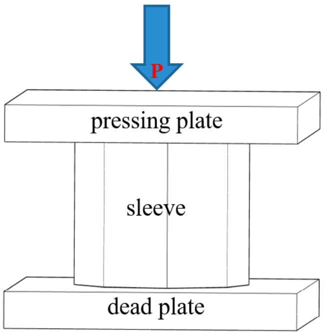

(b) Schematic diagram of sleeve compressive bearing capacity test **(c) Compression test diagram of the sleeve**

Fig.25. Compressive bearing capacity test of sleeve.

6.2 Experimental result

When the load is increased to the design value of the bearing capacity of the sleeve, the deformation of the sleeve is shown in Fig.26a. The sleeve has no visible deformation, and the overall shape has not changed. When the load is loaded to twice the design value of the sleeve compression bearing capacity, the deformation of the sleeve is shown in Fig.26b. It can be seen that the sleeve as a whole has no large deformation, only the edge at the center position of the pin hole shows outward expansion traces, and it can still be installed and used generally after unloading. When the load is loaded until the sleeve has a large deformation, as shown in Figure 26c, the load at this time is about 3.14 times the design value of the compression bearing capacity of the sleeve. It can be seen from the figure that the sleeve bulges outward obviously, and the pin hole is flattened, and the failure was overall buckling of the sleeve. The load-displacement curve is shown in Fig.26d. It can be concluded from the curve that when the load reaches the design value of the compression bearing capacity of the sleeve, the sleeve is in an elastic state and meets the design requirements. When the load comes 2 times the design value of the bearing capacity, the slope of the curve changes, and the sleeve yields to some extent, but it still has a high compressive bearing capacity. When the load comes 3.14 times the design value of the sleeve compression capacity, the sleeve still has a certain compressive bearing capacity. Due to the large deformation of the sleeve, it is considered to have reached the ultimate compressive capacity.

(a) Design value of sleeve compression bearing capacity **(b) 2 times the design value of the sleeve compression bearing capacity**

(c) Large deformation occurs when loading to sleeve

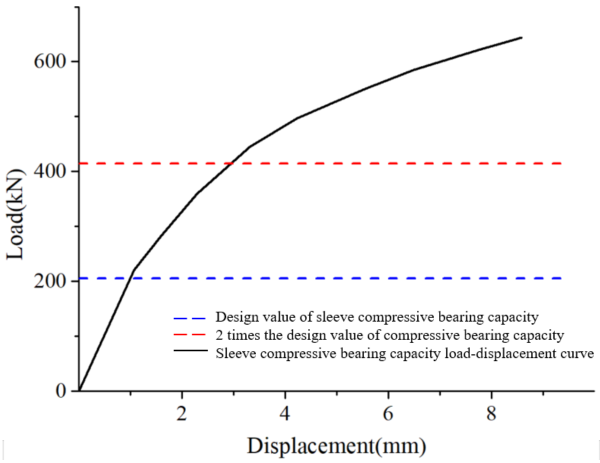

(d) Sleeve compressive bearing capacity load-displacement curve

Fig.26. The test result of sleeve compressive bearing capacity.

7. Sleeve - bolt and pin torsion bearing capacity test

Torsion bearing capacity tests were carried out on the M20 and MY20 with matching sleeves and pins in order to compare the torque that the new and traditional joints can undertake during installation. The test set up follows [19-22]

7.1 Test scheme and device

As shown in Figure 27a, after connecting the sleeve, pin, and the bolt, install the fixture, and turn the sleeve into the fixture along the bolt thread. When the bolt is screwed into the fixture deep enough, the bolt can no longer be screwed due to the restriction of the fixture. Use a digital torque wrench (Fig.27b) to rotate the socket until the pin is cut, and then the torque required to cut the pin can be measured, as shown in Fig.27c. Select two sets of M20 specimens and measure the torque required to shear the pins. Then 2.5 times of the measured torque and the maximum torque that can be applied manually by a single person were loaded into two groups of MY20 specimens to observe the torsional performance and its influence on the pin.

(a) Test schematic of torsional bearing capacity **(b) Digital torque wrench** **(c) Test of torsional capacity**

Fig.27. Torsion test.

7.2 Experimental result

The maximum torque values of the two sets of M20 bolts corresponding to the pins are 73.0N·m and 72.6N·m. The results show that the pin is sheared, and the fracture is a smooth shear surface, as shown in Fig.28a. The pin in the bolt chute is cut into pieces, and the cut pin is difficult to unscrew from the sleeve. There are apparent shear marks at the bolt chute, as shown in Fig.28b. The torque value of 173.4N·m and the maximum manual torque of 306.3N·m was applied to the two groups of MY20 bolts respectively. The results show no change in the pin, and the accessories can be normally disassembled after unloading the force. In the screw part of the bolt, it can be seen that the friction marks left by the contact between the octagonal edge and the inner wall of the sleeve, as shown in Fig.28c and d. The test results show that the new type of joint can bear more than 4 times the torsional bearing capacity of the traditional joint in the installation process and can bear the maximum torque that can be applied by manual labor. The pin can still remain in its original state (Fig.27e), and all parts can be disassembled and used normally after unloading the force.

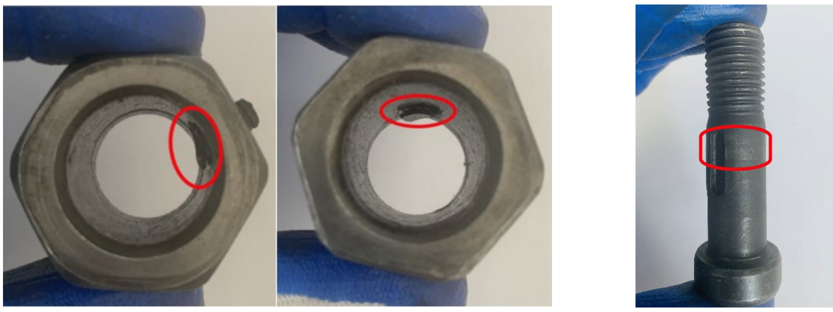

(a) Pin fracture surface **(b) Cut mark in bolt chute**

(c) Friction marks on the inner wall of the sleeve **(d) Friction mark on screw edge** **(e) Pin**

Fig.28. Results of torque test.

8. Numerical simulation

A fine finite element model was established to further study the tensile properties of octagonal high-strength bolts for bolt-ball joints. The accuracy of the finite element model was verified by comparing it with experiments.

8.1 Model set up

The model was established based on ABAQUS. The thread of high-strength bolt has a certain elevation angle along the axial direction of the bolt body. Studies have shown that [23–24] if the thread angle difference is less than 4°, the influence of thread angle on bolt strength can be ignored. The bolt thread angle used in practical engineering is usually less than 4°, so the bolt model does not consider the elevation angle of the thread ring. The refined modeling size was in accordance with the requirements of "General purpose metric screw threads—Basic dimensions" in Chinese (GB/T 196-2003) [25](Fig.29), and the specific size was shown in Table 7. High-strength bolts are made of 40Cr material. The constitutive relation of high-strength bolt and cone head is simplified to a double line model [26], as shown in Fig.30a and b. Stress-strain parameters of steel pipe are obtained from test values, as shown in Fig.30c.

Because the bolted ball joints need to be assembled from different parts, many contacts need to be modeled. In ABAQUS, the possible contact pairs and constraint relationships must be defined. According to "Technical specification for space frame structure" (JGJ7-2010) in Chinese [6], the depth of the bolt into the sphere is greater than 1.1 times the diameter of the bolt. It can be considered that there is no relative sliding between the bolt and the sphere, and binding constraint simulation is selected. The cone head/sealing plate is welded with the member, which is also simulated by binding constraints [27]. Surface to surface contact is selected for the other parts, hard contact is selected for normal contact, penalty contact is selected for tangential connection [28], and the friction coefficient is 0.15[29]. Fig.31 and Table 8 for the contact diagrams between the parts.

One end of the fixture receives constraints in three directions, and the other end exerts a displacement. To ensure the accuracy of the simulation results and the rapid convergence of the calculation, the model is divided by C3D8R three-dimensional solid element [30,31]. Mises stress [32,33] is used as the numerical simulation parameter of the model strength. Fig.32 shows each component and the overall model.

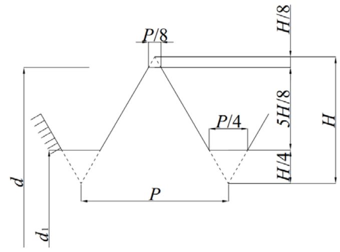

Fig.29. Thread dimension.

Table 7

Thread dimensions of high-strength bolts.

Bolt	*d* (mm)	d_1 (mm)	H (mm)	*P* (mm)
MY20	20	17.294	2.165	2.5
MY36	36	31.670	3.464	4
MY45	45	40.129	3.897	4.5
MY56	56	51.670	3.464	4

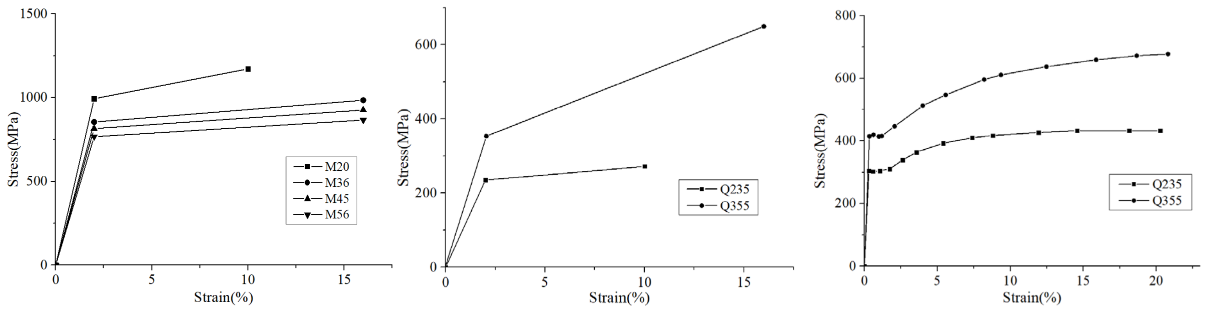

(a) Stress-strain curve of high-strength bolt **(b) Stress-strain curve of cone head** **(c) Stress-strain curve of steel pipe**

Fig.30. Constitutive relation.

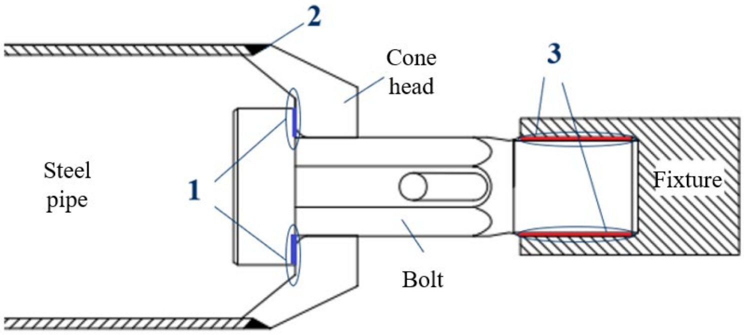

Fig.31. Contact diagram.

Table 8

Model contact settings.

Contact pair number	Description	Contact mode	Interarea faces	Heterotopic faces
1	Nut and cone head	Face to face	Nut	Cone head
2	Member and cone head	Binding	Cone head	Member
3	Thread and fixture	Binding	Fixture	Thread

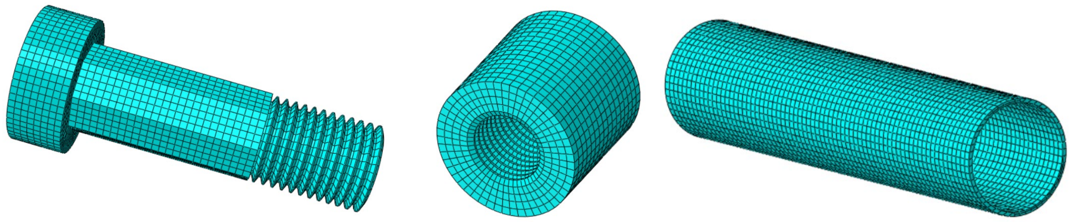

(a) Octagonal high-strength bolts **(b) Fixture** **(c) Steel pipe**

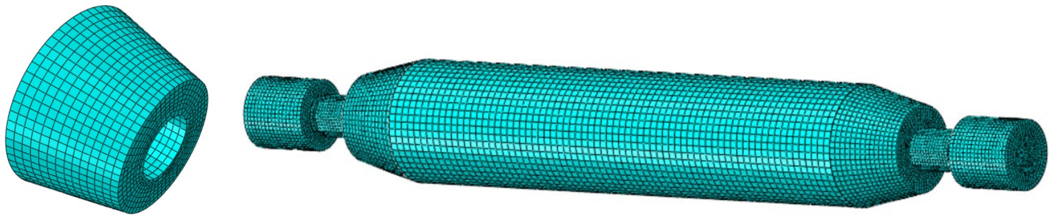

(d) Cone head **(e) Integral assembly model**

Fig.32. Finite element model.

8.2 Tensile simulation result

Fig.33 shows the stress distribution, plastic deformation distribution, and stress distribution at the screw-cone head contact point in the finite element analysis (FEA) of the whole specimen. The high-stress state occurs at the junction of screw and thread (MY20, MY56) and the middle part of the steel pipe (MY36, MY45). The higher plastic deformation in these areas makes the bolt or steel pipe more prone to failure. The plastic deformation of MY56 cone head is larger than that of MY20, and the plastic deformation of MY36 and MY45 cone head is smaller. These characteristics are consistent with the test results. The stress distribution height of the contact part of the nut and the cone head is similar between the traditional bolt type and the new bolt type, indicating that the increase of the hole size of the cone head/sealing plate and the diameter of the nut has little effect on the stress distribution of the contact part and the bearing capacity of the cone head/sealing plate, which is the same as the theoretical analysis results described above.

Table 9 compares the results of the test and simulation, and Fig.34 compares the load-displacement curves of the test and simulation. The following characteristics can be obtained from table 9 and Fig.34: (1) The overall shape and peak point of the load-displacement curve simulated by numerical simulation are in good agreement with the corresponding test curve, indicating that the numerical simulation can accurately estimate the tensile strength of the specimen with an error within ±10%. (2) Compared with the test, the elastic stiffness of the numerical simulation has a slight deviation, and the difference becomes larger with the increase of the bolt type. The reason for the stiffness deviation in the elastic stage is mainly due to the partial slippage between the test bench and the fixture during the loading process [34-35]. The larger the bolt type, the greater the load applied, and the greater the slip between the test bench and the fixture, resulting in a greater difference in elastic stiffness. (3) Fig.34a shows the load-displacement curves of specimens M20—MY20, and Fig.34d shows the load-displacement curves of specimens M56—MY56. Both of them are bolt fracture failures. Fig.34b shows the load-displacement curve of the M36—MY36 specimen, and Fig.34c shows the load-displacement curve of the M45—MY45 specimen. Both are steel pipe fracture and failure, and both show the characteristics of steel pipe ductility.

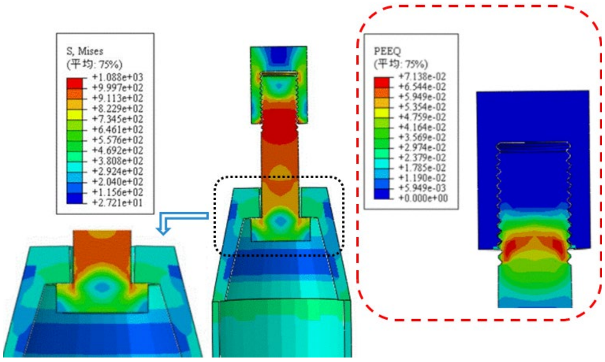

(a) Φ75.5×3.75-MY20

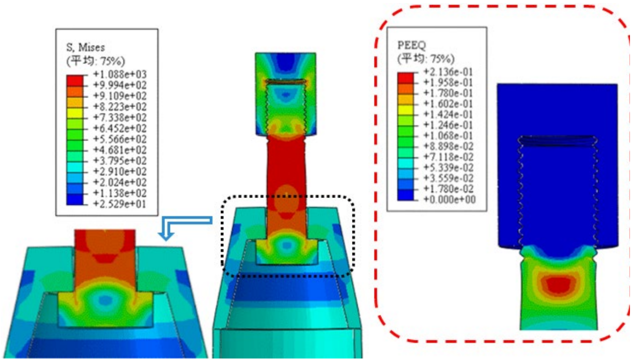

(b) Φ75.5×3.75-M20

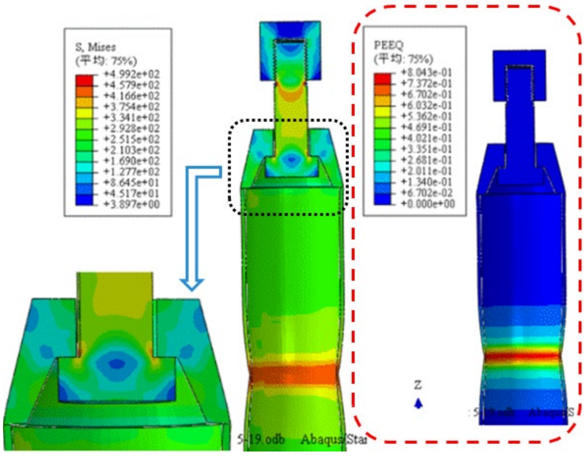

(c) Φ114×4-MY36

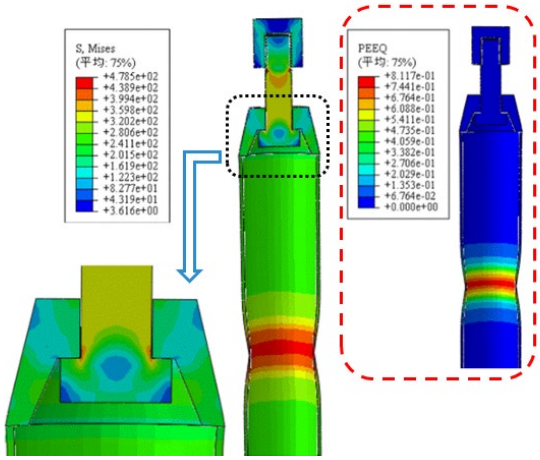

(d) Φ114×4-M36

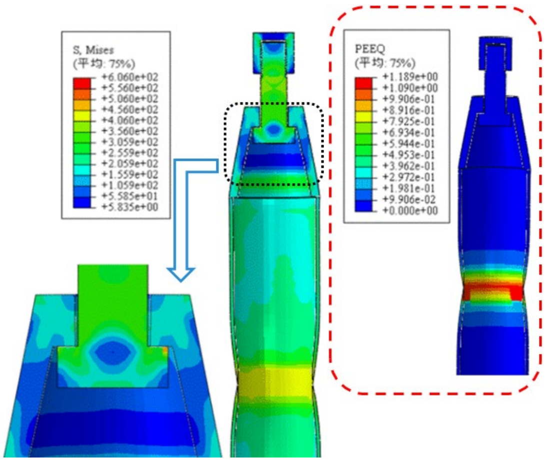

(e) Φ159×6-MY45

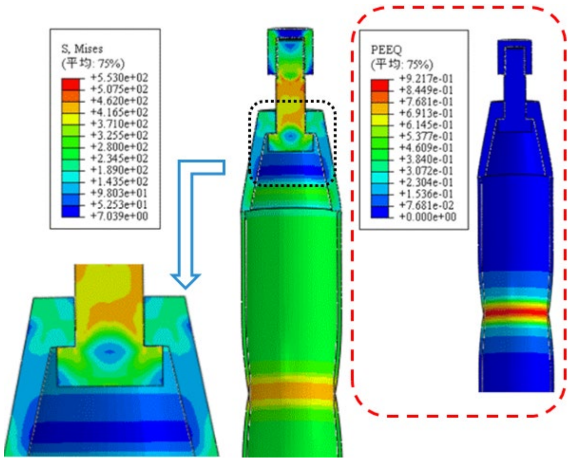

(f) Φ159×6-M45

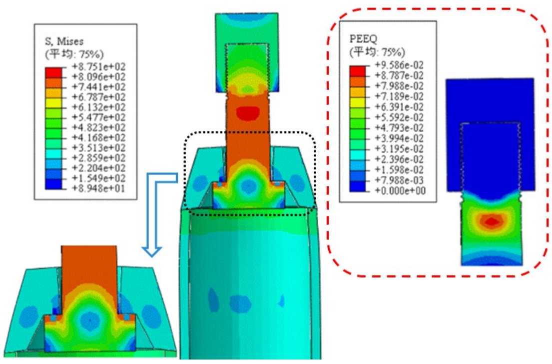

(g) Φ180×12-MY56

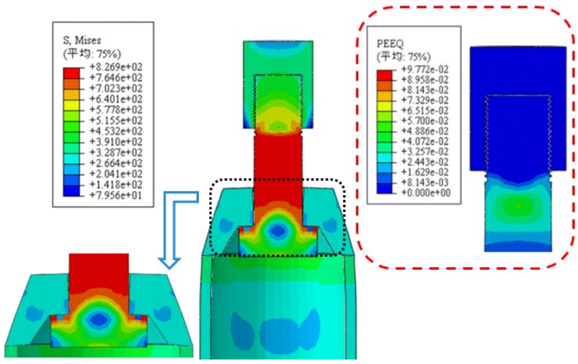

(h) Φ180×12-M56

Fig.33. Finite element analysis results.

Table 9

Comparison of test and simulation results.

Sample type	Test failure mode	Simulated failure mode	Test tensile capacity (average value) (kN)	Simulate tensile bearing capacity (kN)	Error(%)
M20-Φ75.5	Bolt	Bolt	276	298	7.97
MY20-Φ75.5	Bolt	Bolt	288	299	3.82
M36-Φ114×4	Steel pipe	Steel pipe	578	583	0.34
MY36-Φ114×4	Steel pipe	Steel pipe	581	585	0.68
M45-Φ159×6	Steel pipe	Steel pipe	1227	1331	8.47
MY45-Φ159×6	Steel pipe	Steel pipe	1296	1334	2.93
M56-Φ180×12	Bolt	Bolt	2189	2124	-2.97
MY56-Φ180×12	Bolt	Bolt	2192	2157	-1.59

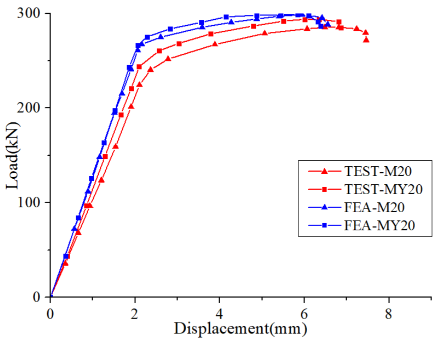

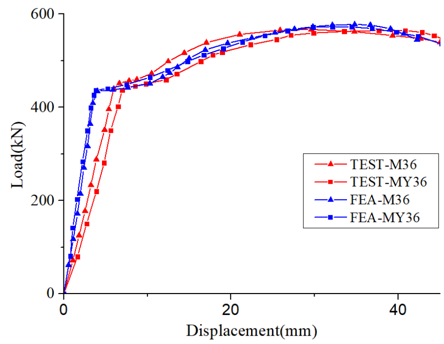

(a) M20—MY20 **(b) M36—MY36**

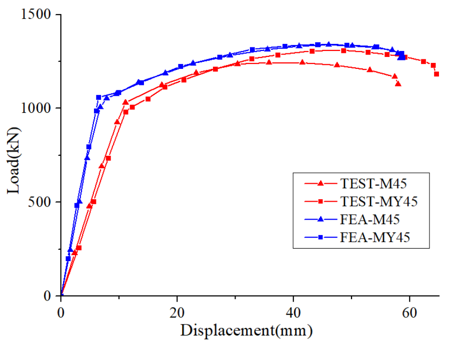

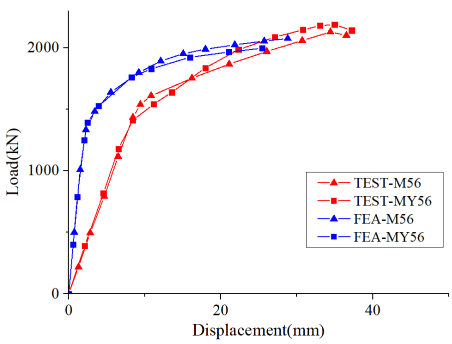

(c) M45—MY45 **(d) M56—MY56**

Fig.34. Load-displacement curves of different types of specimens.

9. Conclusion

Aiming at the "insufficient tightening" phenomenon of high-strength bolts that is common in bolt-ball joints, a new type of bolt-ball joint has been proposed and designed. Explains its anti-false screw mechanism: This node relies on the contact transmission force between the octagonal shape in the sleeve and the octagonal section of the bolt to screw the bolt into the bolt sphere, and the pin is not affected by the shear force, which avoids the pin from shearing. After installation, whether the high-strength bolt is tightened can be directly judged by observing the length of the pin tail exposed to the sleeve surface, which overcomes the disadvantage of "insufficient tightening" of the high-strength bolt in the construction of the traditional bolt-ball joint. The tensile properties of the octagonal high-strength bolts, the tensile properties of the steel pipe-cone head/sealing plate and the whole specimen of the bolt, the bearing properties of the sleeve, and the torsional capacity of the joint installation were studied. The conclusions are as follows:

(1) Four common bolt types, MY20, MY36, MY45, and MY56, were selected to carry out the unidirectional tensile test with 12 octagonal high-strength bolts with 3 samples of each type. The tensile load of one specimen MY45 exceeded the maximum tensile load specified by the standard by 2.36%. The failure load, failure position, failure mode, and elongation of the other octagonal high-strength bolts all meet the requirements of the current standard "High-strength bolts for joints of space grid structures" in Chinese (GB/T 16949-2016).

(2) The tensile test of the whole specimen containing steel pipe—cone head/sealing plate and bolt shows three failure modes, including steel pipe failure, bolt failure, and weld failure. The uniaxial tensile load-displacement curve of the integral test piece containing the steel pipe, cone head/sealing plate, and the traditional high-strength bolt and the integral test piece of the octagonal high-strength bolt is the same, the elastic stiffness is similar, and the plastic load force and ductility are similar. However, the ultimate tensile strength of the octagonal high-strength bolt integral test piece is slightly higher than that of the traditional high-strength bolt integral test piece.

(3) A detailed finite element (FEA) model was established for the whole test piece containing the steel pipe—cone head/sealing plate and bolts for simulation analysis. The analysis results show good consistency with the failure mode and failure load shown in the test, and can clearly show the stress distribution. However, due to the slippage between the test equipment and the fixture, the stiffness of the bolted ball joint cannot be predicted accurately.

(4) The opening size of octagonal high-strength bolts corresponding to the cone head/sealing plate is about 8% more than that of the traditional cone head/sealing plate. Tests and finite element analysis show that the diameter of the octagonal high-strength bolts is designed to be 1mm or 2mm larger than the diameter of the traditional high-strength bolts, which can make the bearing capacity of the new cone head/sealing plate equal to the traditional cone head/sealing plate.

(5) The compression test of the new sleeve shows that its ultimate compressive bearing capacity exceeds its compressive design bearing capacity by more than 3 times.

(6) The torque bearing performance of the new type of joint and the traditional joint during installation is compared through tests. The results show that because the bolt is screwed into the bolt sphere by the contact force of the sleeve and the bolt instead of shear force from the pin, the torque that the new joint can withstand during the installation process is much greater than that of the traditional joint.

10. Acknowledgements

This research was supported by a research grant provided by the Natural Science Foundation of Shandong Province of China (No.ZR2019MEE042) and Key Laboratory of Building Structural Retrofitting and Underground Space Engineering (Shandong Jianzhu Un iversity), Ministry of Education. Any opinions, findings and conclusions expressed in this paper are those of the writers and do not necessarily reflect the view of the funder.

References

[1]A. Hanaor. A Summary Survey of Prefabricated Spatial Frame Systems, J. International Journal of Space Structures. 10(3) (1995) 175-186.

[2] O. Caglayan, E. Yuksel. Experimental and finite element investigations on the collapse of a Mero space truss

roof structure - A case study, J. Engineering Failure Analysis. 15(5) (2007) 458–470.
[3] X.L. Liu. Summary of spatial structure nodes at home and abroad , A. Proceedings of the ninth Conference on Space Structures. (2000) 19-27 (in Chinese).
[4] M. Setareh, B. Jones, L. Ma, et al. Application and Evaluation of Double- Layer Grid Spatial Structures for the Engineering Education of Architects, J. Journal of Architectural Engineering. 21 (3) (2015) 04015005.
[5] K.A. Kounoudji, M. Renouf, G. Mollon, et al. Role of Third Body on Bolted Joints' Self-Loosening, J. Tribology Letters. 61(3) (2016) 1–8.
[6] JGJ 7-2010, Technical specification for space frame structures, China Building Industry Press, Beijing, 2010 (in Chinese).
[7] L.Y. Jiang, X.L. Liu. Analysis of a space truss collapsing in Tian Jin, J. Spatial Structures. 1(3) (1997) 62-64 (in Chinese).
[8] Y.Q. Shi, S.W. Liu, Q.P. Li, et al. Analysis and treatment of grid accident in the lecture hall of science and technology building of a medical college in Shanxi Province, C. 10th Academic Conference on Space Structures. (2002) 885-889 (in Chinese).
[9] S. Ma. Experience in applying grid structure to main building roof for power plant, J. Engineering Journal of Wuhan University. 42(S1) (2009) 123-128 (in Chinese)
[10] China Academy of Building Research. The engineering quality and healthy development of grid structure in steam engine house of Xin feng Power Plant, J. Building Structure. 019(12) (2005) 55 (in Chinese).
[11] D.B. Yang，M.J. Li，G.G. Zhou, et al. Visual anti-insufficient tightening bolted spherical joint for spatial grid structures , P. ZL 202020942989.9, 2020 (in Chinese).
[12] B.S. Huang, Y.D. Fu, Y. Chen, et al. Experimental Study on the Depth of High Strength Bolt into Bolt-Sphere Joint, J. Progress in Steel Building Structures. 18(4) (2016) 28–32 (in Chinese).
[13] GB/T 16939–2016, High strength bolts for joints of space grid structures, China Standards Press, Beijing, China (in Chinese).
[14] X.D. Wang, W. Kai, H.B. Liu, et al. Experimental Study on the Mechanical Property of Visual Bolt-Ball Joint System, J. Advances in Structural Engineering. 16(10) (2013) 1749-1762.
[15] H.D. Zhang, Y.J. Chen, X.H. Luo. Theoretical Analysis and Simplified Calculation for Strength of Cone - shaped Connectors in Bolted Spherical Joints, J. Journal of Building Structures. (06) (2001) 36-42.
[16] L.W. Tong, L.Z. Chen, Y.J. Chen, et al. Experimental study on the behavior of large-diameter mero joints of space trusses, J. Journal of China Civil Engineering. 42(5) (2009) 40–45.
[17] Q.Y. Wu, H.J. Wang, H.L. Qian, et al. Effect of insufficient screwing depth of bolt on mechanical behavior of bolt-ball joint and stability of single-layer reticulated shell, J. Engineering Structures. 213 (2020) 110590.
[18] GB 50205-2020, Standard for acceptance of construction quality of steel structures, Standards Press of China, Beijing, Fu, F. Fire induced progressive collapse potential assessment of steel framed buildings using machine learning, Journal of Constructional Steel Research, 2020, 166, 105918
[19] Fu, F., Lam, D., Ye, J. Moment resistance and rotation capacity of semi-rigid composite connections with precast hollowcore slabs, Journal of Constructional Steel Research, 2010, 66(3), pp 452–461
[20] Wang, L., Shen, N., Zhang, M., Fu, F., Qian, K.,Bond performance of Steel-CFRP bar reinforced coral concrete beams,Construction and Building Materials, 2020, 245, 118456
[21] Chen, X., Wan, D.-W., Jin, L.-Z., Qian, K., Fu, F. Experimental studies and microstructure analysis for ultra high-performance reactive powder concrete Construction and Building Materials, 2019, 229, 116924
[22] Xu, M., Gao, S., Guo, L., Fu, F., Zhang, S. Study on collapse mechanism of steel frame with CFST-columns under column-removal scenario, Journal of Constructional Steel Research, 2018, 141, pp 275–286 China (in Chinese).

[23] S. Hashimura, T. Nutahara, K. Kamibeppu. An Influence of Tightening Torque Stored in Tightening Process on Fatigue Strength of Aluminum Bolts, J. Key Engineering Materials. 4700 (2018) 229–34.
[24] E.L. Grimsmo, A. Aalberg, M. Langseth, et al. Failure modes of bolt and nut assemblies under tensile loading, J. Journal of Constructional Steel Research. 126 (2016) 15–25.
[25] GB/T 196-2003, General purpose metric screw threads—Basic dimensions, Standards Press of China, Beijing, China (in Chinese).
[26] Y. Hu, L. Shen, S.D. Nie, et al. FE simulation and experimental tests of high- strength structural bolts under tension, J. Journal of Constructional Steel Research. 126 (2016) 174–86.
[27] X.C. Li, Z.L. Xie, H. Wu. R bending capacity of bolted hub joints for single—layer latticed shell with rectangular stainless steel tubes, J. Low Temperature Architecture Technology. 42(08) (2020) 42-46 (in Chinese).
[28] B. Egan, C.T. McCarthy, M.A. McCarthy, et al. Modelling a single-bolt countersunk composite joint using implicit and explicit finite element analysis, J. Computational Materials Science. 64 (2012) 203-208.
[29] J.-J. Chen, Y.-S. Shih. A study of the helical effect on the thread connection by three dimensional finite element analysis, J. North-Holland. 191(2) (1999) 109-116.
[30] ABAQUS, Standard User's Manual, Hibbitt, Karsson and Sorensen, Inc, (2014).
[31]Fu, F., Lam, D., Ye, J. Modelling semi-rigid composite joints with precast hollowcore slabs in hogging moment region,Journal of Constructional Steel Research, 2008, 64(12), pp 1408 - 1419
[32] Fu, F., Parke, G.A.R. Assessment of the Progressive Collapse Resistance of Double-Layer Grid Space Structures Using Implicit and Explicit Methods, International Journal of Steel Structures, 2018, 18(3), pp 831 - 842
[33] D. Benasciutti. Some analytical expressions to measure the accuracy of the "equivalent von Mises stress" in vibration multiaxial fatigue, J. Journal of Sound and Vibration. 333(18) (2014) 4326–4340.
[34] B.D. Ding, Y.Q. Zhao, Z.H. Huang, et al. Tensile bearing capacity for bolted spherical joints with different screwing depths of high-strength bolts, J. Engineering Structures. 225 (2020) 111255.
[35] F. Hanus, G. Zilli, J.-M. Franssen. Behaviour of grade 8.8 bolts under natural fire conditions—tests and model, J. Journal of Constructional Steel Research. 67 (2011) 1292–8.